Batteries & Supercaps

Research Article
doi.org/10.1002/batt.202500539

Chemistry Europe
European Chemical Societies Publishing

www.batteries-supercaps.org

Understanding Degradation Mechanisms in Water-In-Salt Electrolyte: Part 1—In Depth Soaking Investigation by Means of Multiprobe Techniques of $LiFePO_4$ versus TiS_2

Célia Doublet, Ove Korjus, Marta Mirolo, Jakub Drnec, Vincent Martin, Emmanuelle Suard, Lorenzo Stievano, Lauréline Lecarme, and Claire Villevieille*

Water-based liquid electrolytes for Li-ion batteries offer the promise of improved safety and lower cost, but the energy density remains too low due to the narrow electrochemical stability window of water. Switching to the water-in-salt electrolyte approach appears to be an ideal solution as the electrochemical stability window of water is extended, thereby increasing the overall energy density. To date, despite an increase in electrochemical stability window, hydrogen evolution reaction (HER) and oxygen evolution reaction still occur during cycling, resulting in poor electrochemical performance. Most articles report that this phenomenon is intrinsically related to the change in potential within the cell. In the present work, we carry out a complete surface-to-bulk investigation of two well-known electroactive materials used in the water-in-salt system, $LiFePO_4$ and TiS_2. The aim in this first part is to understand the role of soaking the composite electrode in the water-in-salt electrolyte and to see if degradation occurs prior to any electrochemical measurement. We show that $LiFePO_4$ is a robust material that develops a surface layer rich in LiF, whereas TiS_2 decomposes at the top surface into a mixture of TiO_2/TiS_2 or oxysulfide byproduct.

1. Introduction

The safety of lithium-ion batteries (LIBs) remains a bottleneck in many applications, especially electric vehicles, where this aspect is a mandatory criterion. Replacement of flammable liquid organic electrolytes with a water-based ones was proposed in 1994[1]; Unfortunately, the electrochemical stability window (ESW) of water is extremely narrow (only 1.23 V), resulting in poor electrochemical performance. In 2015, the introduction of water-in-salt electrolytes (WISE)[2] as an alternative to pure aqueous electrolytes for LIBs has revived interest in the development of water-based batteries. In fact, when a lithium salt is used in excess in mass and volume, the activity of free water molecules is greatly reduced, which extends the ESW by inhibiting the oxygen evolution reaction (OER) potential and pushing the hydrogen evolution reaction (HER) potential to a lower potential (from 2.6 to1.9 V vs. Li^+/Li). Such an approach leads to an extension of the ESW up to 3 V, not far from commercial LIBs.

To date, lithium bis(trifluoromethanesulfonyl)imide (LiTFSI) has been the most studied salt due to its high solubility and stability in water.[3] Based on 21 m (mol.kg^{-1}) LiTFSI WISE, $LiMn_2O_4/Mo_6S_8$ and $LiFePO_4/Mo_6S_8$ full cells were able to achieve up to 1000 cycles with good capacity retention.[2,4] To further improve the electrochemical performance, researchers have developed several strategies for this system, such as combining different salts to further enhance and stabilize the ESW. Yamada et al. demonstrated a complete 3.1 V cell using $Li_4Ti_5O_{12}$ as the negative electrode in a mixed aqueous LiTFSI—LiBETI (lithium bis(pentafluoroethylsulfonyl)imide) electrolyte.[5] Zhang et al.[6] investigated TiS_2 as an electrode material for aqueous batteries in a moderate (2 m LiTFSI) electrolyte concentration, finding that water caused significant degradation. However, they did not examine the effects of higher salt concentrations on this process.

Other groups have reported multiple issues that lead to severe electrochemical degradation during cycles and irreversible damage. For instance, the WISE system suffers from water consumption ("drying out" process), self-discharge, multiple parasitic reactions, pH evolution, and corrosion (both from the casing and the current collector),[7–9] resulting in poor electrochemical

C. Doublet, V. Martin, L. Lecarme, C. Villevieille
Université Grenoble Alpes
Univ. Savoie Mont Blanc
CNRS
Grenoble INP
LEPMI
38000 Grenoble, France
E-mail: claire.villevieille@grenoble-inp.fr

O. Korjus, E. Suard
Institut Laue Langevin (ILL)
Avenue des Martyrs, 38000 Grenoble, France

M. Mirolo, J. Drnec
European Synchrotron Research Facilities (ESRF)
Avenue des Martyrs, 38000 Grenoble, France

L. Stievano
ICGM
Univ. Montpellier, CNRS
ENSCM
34293 Montpellier, France

Supporting information for this article is available on the WWW under https://doi.org/10.1002/batt.202500539

performance. Some of the problems are also related to the nature of the solid electrolyte interphase (SEI). In theory, a high LiTFSI concentration should produce a nonconductive fluorine-based SEI on the negative electrode,[2] which inhibits the HER reaction and thus contributes to the enlargement of the ESW. On the positive electrode side, the salt anions aggregate to form a hydrophobic double layer, buffering the activity of the water molecules, which can no longer undergo the OER. This mechanism reduces the damage that causes poor electrochemical performance.[10–12] However, so far, this has not been the case, as the SEI appears to dissolve in the presence of free water molecules[13] and is therefore not protective enough to suppress OER and HER. The formation mechanism and exact composition of the SEI are still debated in the literature,[9,14–16] with some describing it as mainly composed of LiF, CF_x species, and LiOH, while others claim it is a lithium salt precipitate.

Surprisingly, all related studies in the literature have been carried out on cycled cells. This has led us to conclude that the interfacial layers caused by electrolyte decomposition are driven by the potential evolution occurring inside the cell. However, surface reactions could occur before any electrochemical cycle, once the electrolyte is in contact with the composite electrode. This means that the decomposition observed during cycling could be caused by an earlier decomposition that occurred before any electrochemical activity and developed only by soaking.

In this study, we conducted a full in-depth investigation, using bulk and surface techniques, to verify the stability of the electrode in contact with the electrolyte to guide further research on WISE. To this end, $LiFePO_4$ and TiS_2 composite electrodes were soaked in several WISE concentrations (LiTFSI salt), and their surface was analyzed by X-ray photoelectron spectroscopy (XPS), revealing the development of a surface layer. Additional experiments were carried out to understand the effect of the soaking process on the structure of the materials using X-ray diffraction (XRD), ^{57}Fe Mössbauer spectroscopy, neutron powder diffraction and X-ray absorption spectroscopy (XAS). Finally, electrochemical tests in organic-based electrolytes of soaked and unsoaked electrodes show that the passivation layer developed during the soaking process protects the electrode from further decomposition.

2. Understanding Degradation Processes in Water-in-Salt System

As noted earlier, water-in-salt systems experience significant degradation during cycling, primarily due to electrochemical processes, while chemical degradation is less studied. This work presents a two-part study: Part 1 investigates the electrode/electrolyte interface before cycling, and Part 2 analyzes degradation during cycling with operando techniques. **Figure 1** summarizes this approach.

In both manuscripts, we employed multiple characterizations techniques from bulk analysis to surface analysis to get the full picture of the decomposition at the electrode and electrolyte levels. The first part of this study is dedicated to the investigation of the chemical degradation occurring between the electrode and electrolyte during soaking.

3. Soaking Process

The electrode disks (or powders) are soaked in 1 mL of the solution of choice for 24 h. At the end of the soaking process, the electrode (powder) is rinsed with Milli-Q ultrapure water and

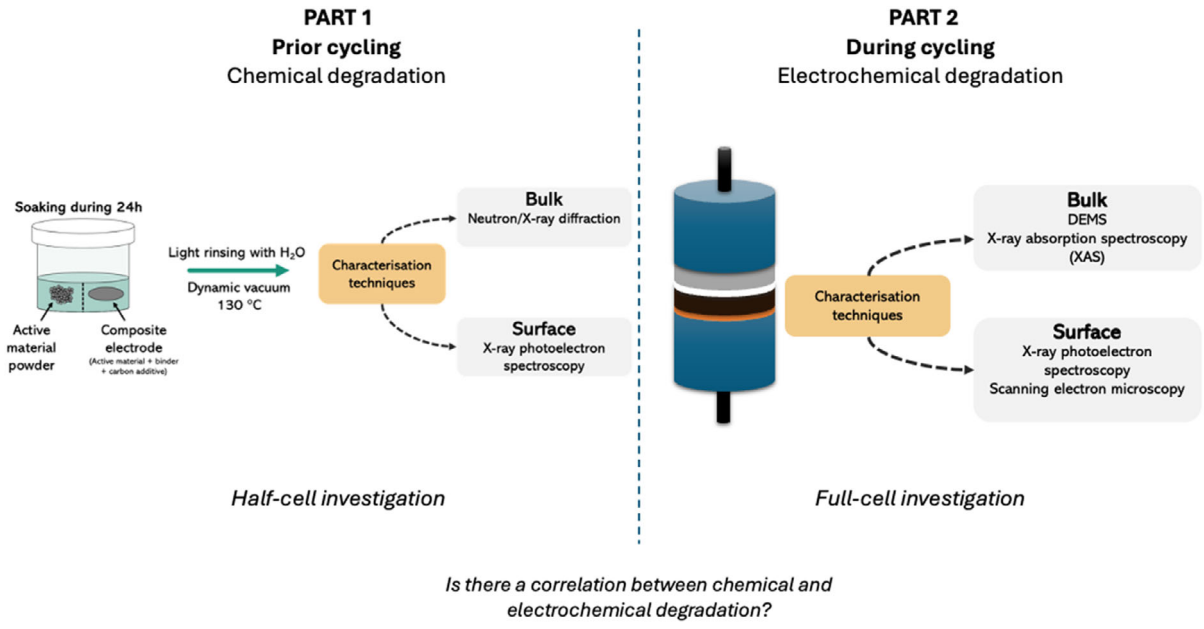

Figure 1. Scheme explaining the complementary between the Part 1 and Part 2 articles to understand degradation processes occurring in water-in-salt system.

Research Article
doi.org/10.1002/batt.202500539
Chemistry Europe
European Chemical Societies Publishing

dried under dynamic vacuum at 120 °C overnight to remove all traces of water. The solutions used for the soaking tests are Milli-Q ultrapure water, 5 m LiTFSI solution, and 21 m LiTFSI solution. As composite electrodes are very complex systems with multiple interfaces, we sometimes used raw materials powder to perform the soaking process experiment to help deconvoluting the impact of binder and carbon additives.

To avoid exposure to air and moisture, the active material powders were stored in an Ar-filled glovebox and exposed to ambient air only during the soaking process.

4. Bulk Characterizations

First, we looked at how the soak process could alter the overall properties of the electroactive materials $LiFePO_4$ and TiS_2 as powders. Once dried, the powders were investigated using X-ray diffraction (XRD) to determine any bulk modification.

4.1. Investigation of Soaked $LiFePO_4$ Powder

Figure 2a shows the XRD patterns of the pristine $LiFePO_4$ powder before and after soaking. No noticeable differences are detected between the two samples, which means that if there are some structural changes, they are below the detection limit of the laboratory diffractometer (less than 2%).

Each diffractogram was fitted with a Le Bail refinement,[17] which refines the lattice parameters *a*, *b*, and *c* as well as other parameters including an average of the full width at half maximum (FWHM) of the diffraction peaks. The refinement of the pristine $LiFePO_4$ powder is shown as an example in Figure S1 (Supporting Information). The fitted parameters presented in Figure 2b and **Table 1** show an evolution of around 1%, indicating that the bulk of $LiFePO_4$ does not appear to be particularly modified by the soaking process. As for the FWHM, it varies from one sample to another very slightly. This behavior may appear surprising at a first glance since the aging (air and water exposure) of $LiFePO_4$ has been reported several times in the literature showing additional phases. Cuisinier et al.[18,19] demonstrated that after 30 days of storage at 120 °C in ambient air, a hydrated form, $Li_xFePO_4(OH)_x$, develops and presents an additional electrochemical plateau around 2.6 V vs. Li^+/Li resulting in poor cycling performance (Coulombic efficiency of 85%). This degradation was found to be reversible, and the active material can recover its full specific capacity after heat treatment.

As XRD is not sensitive to light elements such as Li and H, neutron powder diffraction investigations were carried out at the D2B ILL beamline to determine whether the lithium content changed once the material was soaked. For this purpose, a deuterated LiTFSI solution and deuterated water were used to avoid hydrogen-containing samples, which would make any refinement useless. The neutron diffractograms are shown in Supporting Information Figure S2. The same conclusions are drawn with no noticeable impact of the soaking process on the bulk powder.

Pursuing our bulk investigation, we performed ^{57}Fe Mössbauer spectroscopy to assess the iron oxidation state and coordination chemistry,[20,21] as well as to determine impurities from the synthesis, such as iron phosphide.[22–24] The Mössbauer spectra are presented in **Figure 3**. All samples could be fitted with at least three types of doublets: i) the main one attributed to $LiFePO_4$ doublet (blue, Figure 3a); ii) a broader one, with a little contribution, corresponding to a defective $LiFePO_4$ doublet (red, Figure 3a); and iii) a last one attributed to iron phosphide species, which is a typical contamination in commercial $LiFePO_4$ (yellow, Figure 3a).

When it comes to the Mössbauer measurements, a very small difference is observed between the samples. First, the impact of water or WISE does not change the oxidation state of Fe, which remains Fe^{2+}. To identify possible subtle differences between the samples, we used a nonstandard fitting process, fitting all the spectra together keeping common hyperfine parameters for all components, and allowing only the resonance areas to vary. The resulting fit parameters are reported in Supporting

Table 1. Lattice parameters a, b, and c and the average FWHM extracted from Le Bail refinements of pristine or soaked $LiFePO_4$ powder in water, 5 or 21 m LiTFSI solutions.

Sample	*a* [Å]	*b* [Å]	*c* [Å]	FWHM
Pristine	10.3254(2)	6.0056(1)	4.6930(1)	0.177(2)
Soaked in water	10.3262(1)	6.0060(1)	4.6934(2)	0.172(1)
Soaked in 5 m	10.3268(2)	6.0063(1)	4.6935(1)	0.176(2)
Soaked in 21 m	10.3268(1)	6.0061(1)	4.6935(2)	0.174(1)

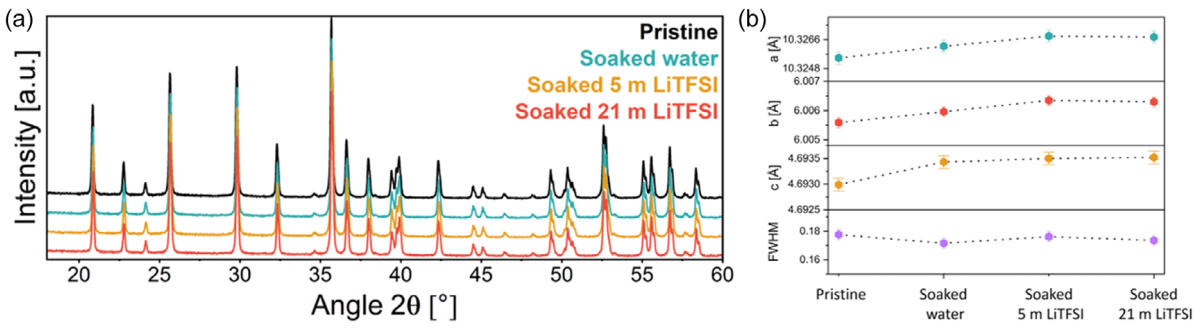

Figure 2. a) XRD diffractograms of pristine powder of $LiFePO_4$ active material (black), after soaking in water (blue), 5 m LiTFSI solution (yellow), and 21 m lITFSI solution (red). Data were collected using a Cu K_α source $\lambda_{(Cu\ K\alpha)} = 1.5406$ Å; b) Lattice parameters a (green), b (red), c (yellow), and mean FWHM (purple) extracted from Le Bail refinements.

Research Article
doi.org/10.1002/batt.202500539
Chemistry Europe
European Chemical Societies Publishing

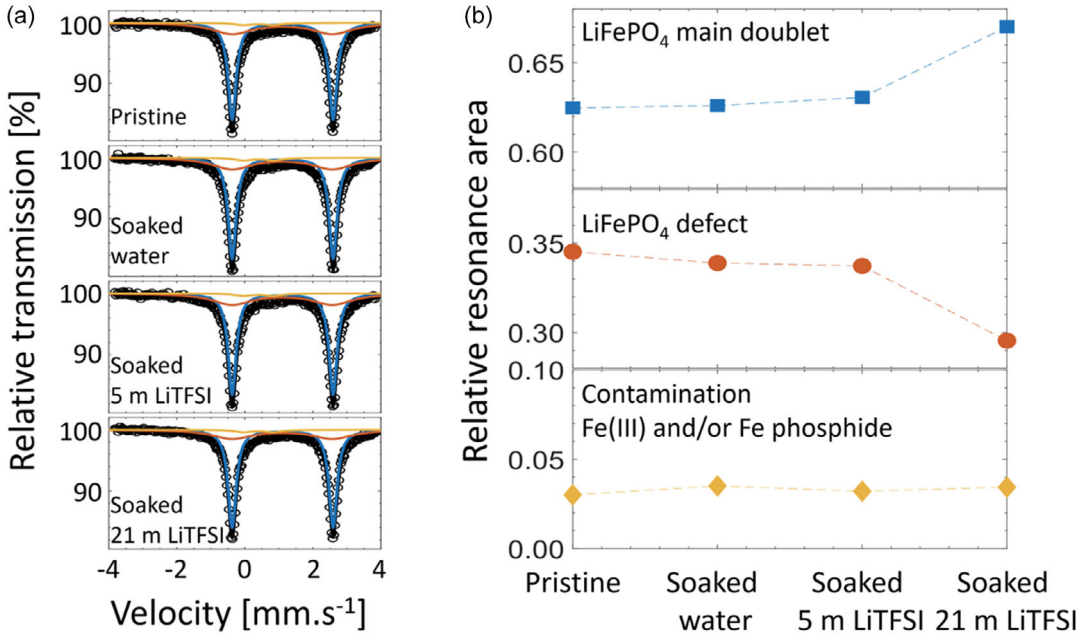

Figure 3. a) ^{57}Fe Mössbauer spectra of $LiFePO_4$ active material powder pristine, after soaked in water, 5 and 21 m LiTFSI solution. b) Results from the fitting of the relative resonance area for each Mössbauer spectrum.

Information, Table S1. The isomer shift scale is referred to α-Fe at room temperature. The relative resonance areas of the three components are presented in Figure 3b for each sample. The doublet representing Fe^{3+} and/or iron phosphide species does not change much from one sample to another, meaning that impurities are not affected by any soaking process. However, surprisingly, soaking the sample leads to an increase of the relative resonance area for the main $LiFePO_4$ doublet, whereas simultaneously, the defective one decreases. This process is particularly visible in the sample soaked with a 21 m LiTFSI solution. The meaning of such behavior is, to date, unclear, as the contribution of defective $LiFePO_4$ is not reported in the literature and could be due to Li/H exchange.

All these results, obtained from XRD, NPD, and Mössbauer spectroscopy, carried out on $LiFePO_4$ powder, show that the soaking process has little or no impact on bulk properties. A similar investigation was conducted on the TiS_2 material, which we will use as a negative electrode material.

4.2. Investigation of Soaked TiS_2 Powder

We used the same method to study TiS_2 powder, using X-ray and neutron powder diffraction to understand how soaking affects the bulk properties.

Figure 4a shows the XRD patterns of the TiS_2 pristine and soaked active material measured at the ID31 beamline at ESRF. Rietveld refinement was performed on synchrotron data for all TiS_2 powder, and an example of the pristine sample is given in the Supporting Information in Figure S3. The Rietveld refinement is not ideal, which is due to the incomplete occupancy of sulfur atoms, most likely caused by the impact of air/moisture on the sample. Nevertheless, the fitted parameters for each sample are presented in Figure 4b and **Table 2** as a function of their soak history. The lattice parameters do vary significantly with the soaking process, especially the *a* and *b* lattice parameters (in plane). On top of the lattice variation, we can see that the sulfur occupancy decreases as a function of water content; the worst

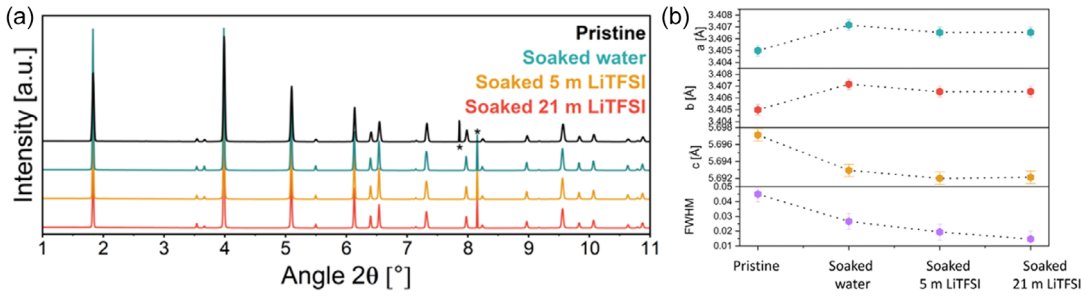

Figure 4. a) XRD diffractograms of TiS_2 active material pristine powder (black), after soaked in water (blue), 5 m LiTFSI solution (yellow) and 21 m LiTFSI solution (red). $\lambda = 0.1822$ Å. "*" indicates peak from the sample holder; b) Lattice parameters *a* (green), *b* (red), *c* (yellow), and the average FWHM (purple) extracted from the Le Bail refinements.

Table 2. Lattice parameters *a*, *b*, *c*, and the average FWHM extracted from the Rietveld refinements of pristine or soaked TiS_2 powder in water, 5 or 21 m LiTFSI solutions.

Sample	*a* [Å]	*b* [Å]	*c* [Å]	FWHM	S occ.
Pristine	3.40449(6)	3.40449(6)	5.69735(15)	368(1)	97%
Soaked in water	3.40790(6)	3.40790(6)	5.70139(15)	250(1)	91%
Soaked in 5 m	3.40718(6)	3.40718(6)	5.70030(15)	260(1)	92%
Soaked in 21 m	3.40725(1)	3.40725(1)	5.69974(13)	247(1)	97%

samples were the one soaked in water and the one with moderate concentration (5 m). This behavior is to put in perspective with the immersion of TiS_2 powder in water that leads to the production of gas, likely H_2S (see Article Part 2).

An attempt was made in the Rietveld refinement to compensate for the missing sulfur occupancy by oxygen, since oxysulfide materials are quite often reported in the literature.[25] Indeed, TiS_2 reacts with air and water, resulting in the loss of sulfur and the formation of oxysulfides, as described by (Equation 1) and (Equation 2). Martinez et al.[25] reported that when TiS_2 is left in contact with air, it can form a surface layer made of TiO_2 while releasing H_2S.

$$TiS_2 + O_2 \leftrightarrow TiS_{2-x}O_x + x/4\,S_8 \quad (1)$$

$$TiS_2 + x\,H_2O \leftrightarrow TiS_{2-x}O_x + x\,H_2S \quad (2)$$

Surprisingly, the sample soaked in the highest concentration of water-in-salt, 21 m, is similar to the pristine sample, meaning that high salt concentration, the activity of water decreases and that the sample tends to be protected by high salt content.

Additionally, we notice that the crystallites size decreases once the TiS_2 is a contact with a water or water-in-salt meaning that TiS_2 is altered by the soaking process, leading to an amorphization of particles, with most probably a surface being oxygen-rich (see XPS part) and the bulk remaining sulfur-rich.

As it was demonstrated in the literature that water can intercalate inside TiO_2,[26] we performed an in-depth investigation using neutron powder diffraction and deuterated solutions. Unfortunately, the powders were stored in ambient air for a short period prior to being measured, compared with the XRD investigation. We still present here the results acquired, and, for the sake of clarity, we will only discuss hypotheses. Figure S4a (Supporting Information) presents the resulting neutron diffractograms. Thanks to the Rietveld refinement performed on these samples, we identified that TiS_2 is the main phase alongside TiO_2 as an impurity, indicating that once again, TiS_2 is extremely sensitive to storage condition since 3% of sulfur atoms are substituted by oxygen, on the top of TiO_2, indicating the formation of an oxy-sulfur phase. Surprisingly, three Bragg peaks located between 38 and 42° could not be fitted properly (Figure S4b, Supporting Information). The reason is that these reflections are extremely broad compared with the other reflections, making the refinement difficult. As the sample was stored in air, we first suspected the reaction of moisture with the sample. However, hydrogen in a sample will lead mostly to an incoherent scattering increasing the background but cannot influence the peaks in such a manner, especially that we are expecting a surface effect; thus, the amount of hydrogen cannot explain the observed peak intensity. Furthermore, when the sample is immersed in D_2O, similar observations are made except that the intensity of these peaks increased drastically (Figure S4c, Supporting Information). The broadening of these three reflections can then be attributed to either TiO_2 and/or TiO_xS_y phases most probably located at the surface of TiS_2 and not properly ordered (kind of amorphous surface layer generated by contact with air/moisture). One cannot exclude also a hydrated TiS_2 phase, to date. Additionally, the substitution of sulfur by oxygen, in TiS_2 lattice, increases to 7% occupancy, showing that water drastically impacts the structure of TiS_2, leading to TiO_2 and TiO_xS_y impurities. For the powder soaked in 21 m LiTFSI D_2O solution, the rinsing procedure was not fully effective resulting in the presence of crystalline Bragg reflection ascribed to salt residue.

At this stage, and based on combined XRD and NPD data, a large amount of salt seems to buffer the reaction of TiS_2 with water (since the number of free water molecules is also reduced), the reasons being: i) we visually observed a reduced gas production at high salt concentration (almost no bubbles formed at the surface of the powder); ii) since the amount of water decreases with increasing salt concentration, there should be less "free" water reacting with TiS_2,; iii) TiS_2 lattice parameters are preserved when soaked in 21 m LiTFSI D_2O solution and enlarged when soaked in H_2O/D_2O. These observations are supported by the previous results of Sun et al.[27] who, after 30 days of soaking TiS_2 in a 21 m LiTFSI solution, did not observe any noticeable difference by XRD, indicating that the high salt concentration could mitigate the water degradation reaction.

In summary, the reactions observed with water/WISE reveal a high reactivity of TiS_2 in aqueous solutions with moderate salt concentrations, contrary to $LiFePO_4$, which appears to be more stable. We pursued our investigation by looking at the surface of the electrodes subjected to the same soaking procedures.

5. Surface Characterization of the Electroactive Materials Powder

We first investigated the electrode materials as powder forms to simplify the system before investigating the composite electrode. The results gathered in section 5.1 and 5.2 will help guide the discussion in section 6(composite electrode).

5.1. $LiFePO_4$ Powder

Figure 5 displays the C1s, Fe2p, and O1s XPS core level spectra of the $LiFePO_4$ powder, in the pristine state and soaked in different electrolyte solutions. The peak positions are summarized in Supporting Information, Table S2. The C1s core level spectrum (Figure 5a) presents three main contributions, the C—C bond at 284.8 eV (black), which is used to calibrate the data and is

Research Article
doi.org/10.1002/batt.202500539
Chemistry Europe
European Chemical Societies Publishing

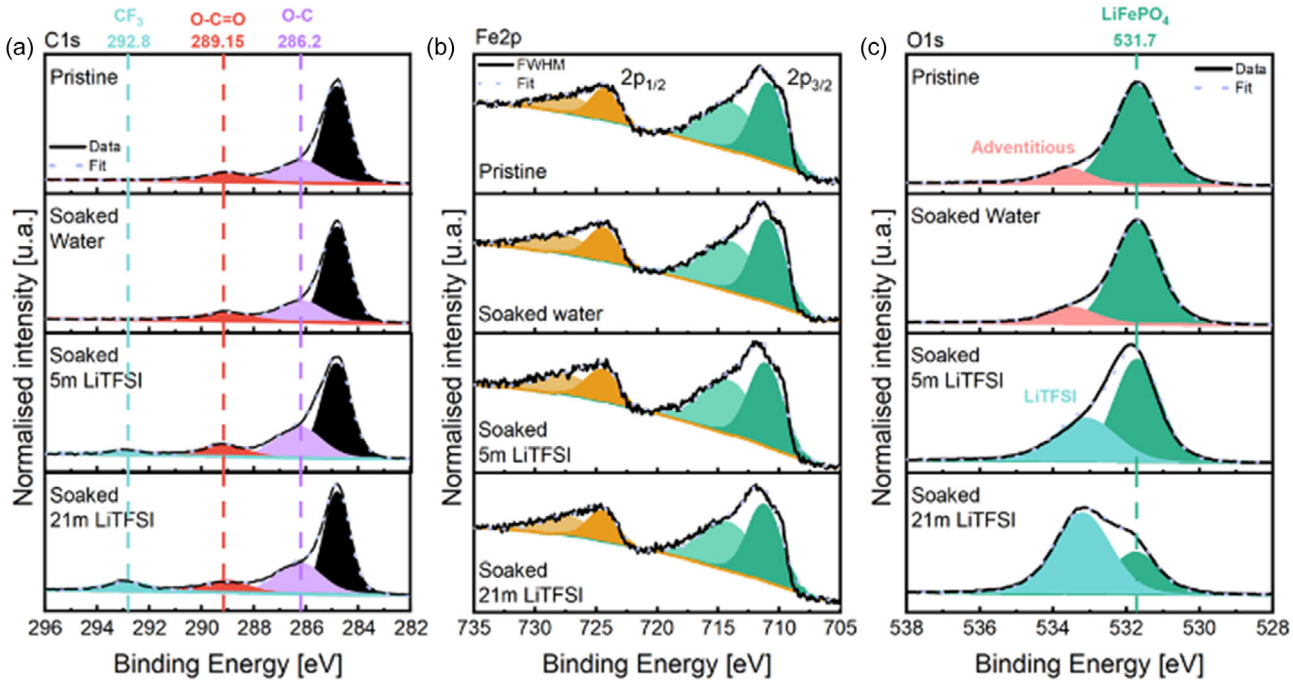

Figure 5. XPS core level spectra of a) C1s, b) Fe2p, and c) O1s obtained from $LiFePO_4$ pristine powder and soaked in water, 5 m LiTFSI solution or 21 m LiTFSI solution.

related to carbon coating of the powder: the C—O bond at 286.2 eV (purple) and O—C═O bond at 289 eV (red). Adventitious carbon species (purple) are almost always present on the surface of samples exposed to air/moisture, and often even on those stored under vacuum.[28] The O—C═O bond could correspond to lithium carbonate Li_2CO_3, as this species is always present at the surface of materials containing lithium and is generally obtained through exposure to air/moisture, even shortly.[29] As for the Fe2p core level spectrum (Figure 5b), it displays four contributions, divided into two spin–orbit doublets: The first one has a 2p3/2 contribution at 710.8 eV and the corresponding 2p1/2 one at 724.3 eV. Their binding energy indicates that iron is in the oxidation state $+2$[30,31] in agreement with Mössbauer spectroscopy. The two additional contributions at 714.0 and 727.3 eV are the so-called satellite peaks. Finally, on the O1s core level spectra (Figure 5c), we can notice only two contributions; one is associated to $LiFePO_4$ itself (oxygen of the PO_4^{3-} group) at 531.7 eV (green) and the other one is most likely related to lithium carbonate species at 533.6 eV as seen on C1s core level spectrum.

Figure 5 shows how the XPS core level spectra of $LiFePO_4$ powder change when soaked in water or in WISE. The resulting spectra are fitted accordingly to the fit presented for the pristine. As can be seen on C1s and O1s core levels (Figure 5a,c), soaking in water surprisingly does not alter the sample surface.

However, soaking in LiTFSI solutions results in an increase of C-O contribution on C1s core level spectrum. Furthermore, a new contribution arises, caused by salt residues, characterized by -CF_3 contribution at 292.8 eV. In the O1s core level spectrum, a contribution at 533.1 eV is also ascribed to LiTFSI salt residue (-S═O). However, we cannot rule out the possibility of adventitious carbon species on the O1s core level spectrum that could be due to the hygroscopic nature of LiTFSI. To confirm this last hypothesis, the LiTFSI salt, stored in a glovebox, was dried under vacuum prior to being measured with XPS to verify its hygroscopic nature. The resulting C1s, F1s, and O1s core level spectra can be found in Supporting Information, Figure S5. On the C1s core level spectrum, a large contribution from C—O can be seen although the salt was stored in a glovebox and was never in contact with ambient air.

Thus, this slight increase in the $LiFePO_4$ sample soaked in WISE is probably due to salt residue. Regarding the Fe2p core level spectrum (Figure 5b), the ratios and intensities are the same from one sample to another, indicating that the soak process has no appreciable effect on the material itself, neither on the bulk nor on the surface.

To conclude, the soaking process has a very limited impact on $LiFePO_4$ powder.

5.2. TiS_2 Powder

Figure 6 displays the C1s, Ti2p, and O1s XPS core level spectra of TiS_2 pristine powder (the S2p core level spectrum is displayed in Supporting Information, Figure S6). The peak positions are summarized in Supporting Information, Table S4. The C1s core level spectrum (Figure 6a) presents three contributions, corresponding to C—C bonds at 284.8 eV, used to calibrate the data, and the adventitious C—O and O—C═O species at 286 and 287.8 eV respectively. As for the Ti2p core level spectrum (Figure 6b), we can observe two spin–orbit doublets, the first one representing TiS_2 at 462.3 and 456.2 eV, and the other one typical of TiO_2 at

Research Article
doi.org/10.1002/batt.202500539
Chemistry Europe
European Chemical Societies Publishing

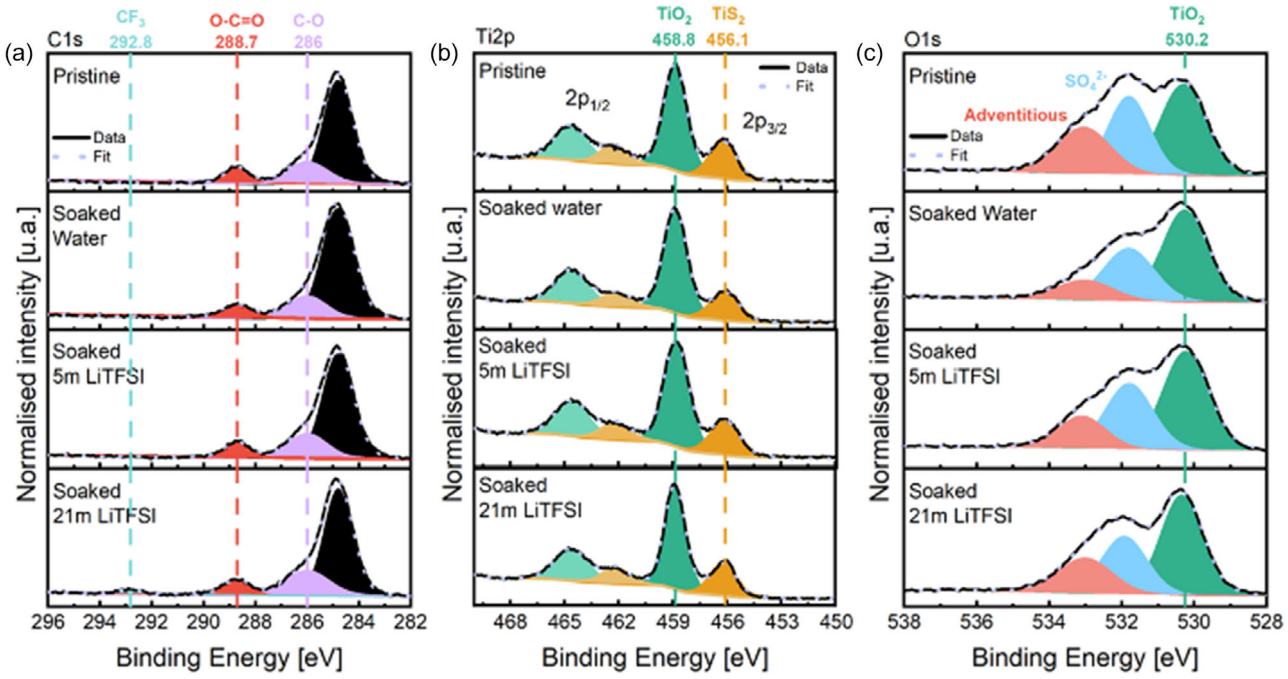

Figure 6. XPS core level spectrum of a) C1s, b) Ti2p, and c) O1s obtained from TiS_2 powder pristine and soaked in water, 5 m LiTFSI or 21 m LiTFSI solutions.

458.9 and 464.6 eV.[25,32,33] This shows that a small amount of TiO_2 is formed at the surface of the TiS_2 particles, even if the sample was carefully protected from air exposure. Considering the probing depth of the XPS instrument (using a standard Al K_α source) and based on the relative amounts of TiS_2 and TiO_2, the thickness of the TiO_2 layer can be estimated at less than 10 nm, probably of the order of 6 to 7 nm.

The O1s core level spectrum (Figure 6c) exhibits three contributions, one associated to TiO_2 at 530.6 eV, another with SO_4^{2-} at 532.1 eV and the last at 533.4 eV corresponding to adventitious C—O species. The contribution at 532.1 eV suggests a moisture contamination at the particle surface,[32] confirming the strong reactivity of TiS_2 with minimal amount of air/moisture.

Soaking the sample in water or electrolyte solutions does not have an effect on the C1s core level spectra (Figure 6a), except for the appearance of a weak contribution of CF_3 on the sample soaked in the 21 m LiTFSI solution, which represents a salt residue.

From the Ti2p core level spectra (Figure 6b), we calculated the TiO_2/TiS_2 peak area ratio. The pristine powder shows a ratio of 2.5, the one soaked in water 3.1, soaked in 5 m LiTFSI solution 2.8, and soaked in 21 m LiTFSI solution 2.5. As expected, soaking TiS_2 in water leads to an increase of the contribution from TiO_2 due to the high reactivity of TiS_2 to water molecule. When the salt concentration increases, the ratio is comparable to that obtained for the pristine powder. This behavior indicates that increasing the salt concentration and thus decreasing the free water activity reduces the reactivity towards TiS_2. Regarding the O1s core level spectra (Figure 6c), no major difference is observed. S2p core level spectra are given in Supporting Information, Figure S6, and support previous statement.

The reactivity of TiS_2 is rather large at the bulk and surface level, which might have an impact on the electrochemical performance. Indeed, TiO_2 has a working potential below that of TiS_2, which could bring the electrochemical activity of the negative electrode closer to HER (See article Part 2). Once HER is reached, it will lead to water consumption (dryness of the system) and might lead to the release of polysulfides in the solution, resulting in a drastic decrease in the overall electrochemical performance of the cell.

6. Surface Characterization of the Composite Electrode

We performed the same experiment on composite electrode materials (composed of electroactive material, a binder, and conductive agent) to determine if an interphase could be developed at the surface of the composite electrode prior electrochemical cycling.

The composite electrodes follow the same soaking protocol of the powders, the rinsing procedure consisting in dipping once the electrode in a vial full of deionized water. The electrodes are then dried overnight at 120 °C under dynamic vacuum prior to XPS investigation.

6.1. $LiFePO_4$ Composite Electrode

First, we analyzed the XPS spectra of the pristine composite electrode as a reference. To better ascribe the contributions of the different electrode components (especially that of the binder),

a reference film of PVDF HSV900 was measured in the same conditions (Figure S7, Supporting Information). The peak positions are summarized in Supporting Information, Table S2 and S3.

6.1.1. Pristine Composite Electrode

In the C1s core level spectrum (**Figure 7**a), several contributions are visible: The first one, corresponding to C–C species at 284.8 eV, mainly derives from carbon Super P and $LiFePO_4$ carbon coating. This contribution is used for the calibration of all spectra. Then, we noticed the presence of adventitious carbon species and lithium carbonate located around 286.1 (C—O), 287.8 (C═O) and 288.8 eV (O—C═O), as measured on the pristine powder. Finally, two peaks can be observed at 290.9 and 286.6 eV, both attributed to PVDF binder. Indeed, as shown in the C1s core level spectrum of the binder (Figure S7, Supporting Information), these two contributions represent respectively $-CF_2$ and $-CH_2$ species[34] and are fitted with the same surface area ratios due to their common origin.

The F1s core level spectrum (Figure 7b) has two contributions, the most intense one at 688 eV is attributed to the $-CF_2$ groups coming from the binder, in good agreement with the measurement performed on reference binder film (Figure S7, Supporting Information). A second, very weak contribution, around 685 eV corresponds to the inorganic LiF salt. The presence of LiF is rather unexpected, since it may be the result of an uncontrolled contamination or formed during electrode fabrication (a reaction between $LiFePO_4$ and the binder caused by either the NMP solvent and/or the high mechanical energy applied during electrode fabrication (Ultra Turrax)).

Finally, the O1s core level spectrum presents two major contributions, one associated with adventitious carbon species at 533.6 eV, most probably due to storage and air exposure of the active material (formation of lithium carbonate and adsorbed species), and the other coming from the oxygens of the phosphate groups in $LiFePO_4$ at 531.7 eV.

6.1.2. Composite Electrode Soaked in Water

For the electrode soaked in water, the C1s core level spectrum (Figure 7) is similar to that of the pristine electrode, except that the contribution related to lithium carbonate and adventitious carbon species are more intense. This phenomenon can be easily explained by the water adsorbed at the surface of the carbon and the reaction between $LiFePO_4$ and water generating lithium carbonate species.

6.1.3. Composite Electrode Soaked in WISE

For the electrodes soaked in WISE, a new contribution appears at 293.2 eV, assigned to $-CF_3$ from LiTFSI salt residues/precipitation.[35] Regarding the F1s core level spectrum (Figure 7b), pristine and water-soaked electrodes are almost identical, containing mainly the contribution of the PVDF binder. It should be noted that for the electrode soaked in WISE, all peaks are slightly shifted (0.2–0.3 eV) toward higher binding energy due to a charging effect. In the present case, the contribution of LiF has drastically increased compared with pristine and soaked water electrodes, a $-CF_3$ contribution also appearing due to LiTFSI salt residues/precipitation. Both contributions indicate the presence of an

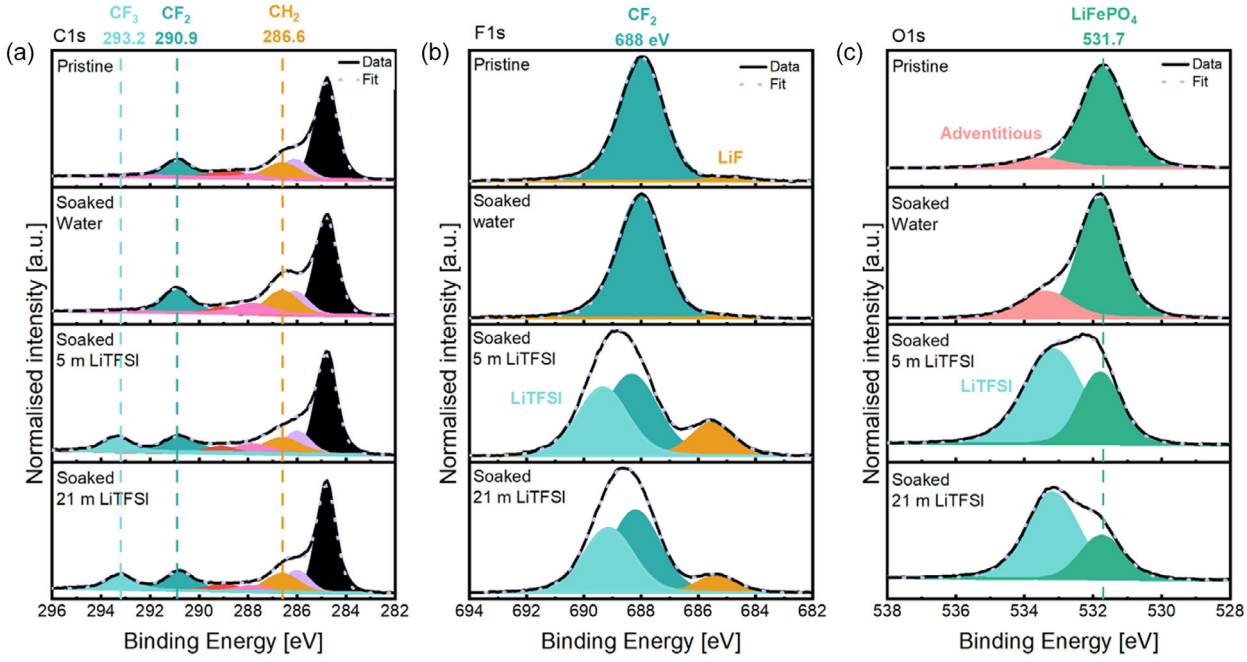

Figure 7. XPS core level spectra of a) C1s, b) F1s, and c) O1s obtained from $LiFePO_4$ composite electrodes, pristine and soaked in water, 5 or 21 m LiTFSI solutions.

insulating surface layer that generates charging effect (due to the lack of electronic conductivity),[36] meaning that surface decomposition may occur also in the absence of an applied electrochemical potential.

At this stage, LiF can have two main origins: i) LiTFSI salt decomposition induced by X-rays (so-called beam damage)[15,16,37,38] and ii) a chemical reaction leading to its formation. For the former, the hypothesis is ruled out since the F1s core level spectrum of the LiTFSI salt (Figure S5, Supporting Information) measured under the same conditions shows a drastically lower amount of LiF. For the second hypothesis, it may come from the electrode fabrication (as discussed for the pristine composite electrode). Indeed, during electrode fabrication, a partial delithiation of $LiFePO_4$ surface is observed due to the reaction between the electroactive material and the NMP solvent (pH around 10).

Figure 8 shows the atomic percent of fluorine species for the different samples. The CF_3/LiF ratio for LiTFSI salt alone is 90/10, whereas it is 38/15 and 41/9 for $LiFePO_4$ composite electrodes soaked in 5 m LiTFSI and 21 m LiTFSI solutions, respectively. It shows that the LiF content increases by soaking the composite electrode in WISE compared with the LiTFSI salt alone. It is surprising that electrode soaked in 5 m LiTFSI solution exhibits the highest LiF content, which could be attributed to rinsing disparities between the WISE-soaked samples.

The O1s core level spectra, displayed in Figure 7c, show similar contributions on pristine and water-soaked electrodes.

For the WISE-soaked samples, the same contributions are observed, although slightly shifted to a higher binder energy by 0.3 eV because of the presence of insulating surface species (especially LiF). An additional contribution corresponding to LiTFSI residues is also observed. For Fe2p core level spectra (Figure S8, Supporting Information), the intensity of the $LiFePO_4$ signal decreases as the concentration in salt increases, indicating that the material is covered by a thin layer, probably containing LiTFSI salt residue and LiF.

6.2. TiS_2 Composite Electrode

A similar investigation was carried out on TiS_2 composite electrodes to see the impact of soaking on the surface composition.

The C1s XPS core level spectrum of the pristine TiS_2 composite electrode is shown in **Figure 9**a. The peak positions are summarized in Supporting Information Table S5. The C–C species are calibrated at 284.8 eV, the binder contributions appear at 286.8 (-CH_2) and 291.4 eV (-CF_2), shifted respectively by 0.2 and 0.5 eV compared with $LiFePO_4$ electrode. This shift can arise from the insulating nature of sulfide materials, especially since they are not carbon coated. Adventitious carbons species are located at 286 eV (C—O) and 288.7 eV (O—C═O). For the electrode soaked in the 21 m LiTFSI solution, we found the same contributions as for the pristine electrode, except that they are slightly shifted (0.2 eV). The contributions from the binder -CF2 (290.8) and -CF3 (293.3 eV) are less visible than in the pristine sample due to a surface layer covering the electrode. LiTFSI salt residues are visible in the samples, similarly to the previously mentioned $LiFePO_4$ electrode.

The contribution of C—O species is largely increased by the soaking in 21 m LiTFSI solution; however, the peak is rather broad and could hide additional contributions. Regarding the Ti2p core level spectrum (Figure 9b), even for the pristine electrode, there is no signal associated with TiS_2 but only with the presence of TiO_2. This is rather surprising since a mixture of TiO_2 and TiS_2 was found in the electrode material powder. A reasonable explanation for such behavior is the chemical reaction of the electrode material with air/moisture and NMP solvent. Indeed, the composite electrodes are elaborated in ambient air and dried in the air; TiS_2

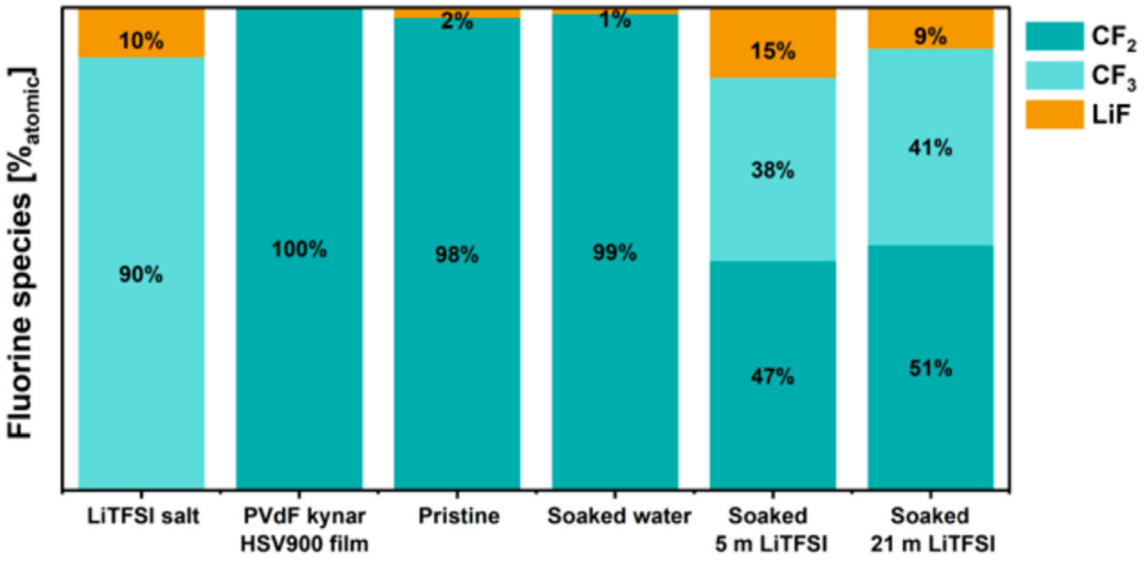

Figure 8. Atomic percentages of fluorine species extracted from the fit of F1s core level XPS spectra of LiTFSI salt, PVDF HSV900 film, pristine $LiFePO_4$ electrode, $LiFePO_4$ electrode soaked in water, $LiFePO_4$ electrode soaked in 5 m LiTFSI solution, and $LiFePO_4$ electrode soaked in 21 m LiTFSI solution.

Research Article
doi.org/10.1002/batt.202500539
Chemistry Europe
European Chemical Societies Publishing

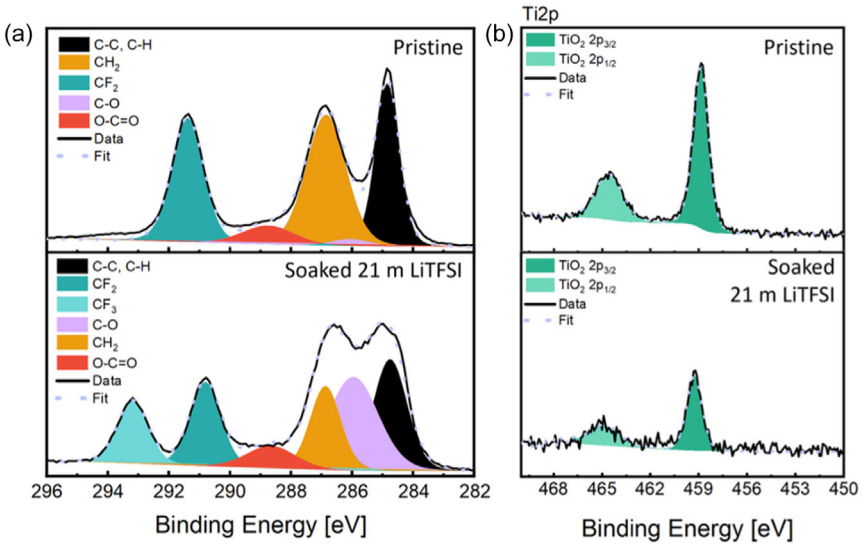

Figure 9. XPS core level spectrum of a) C1s and b) Ti2p obtained from TiS_2 composite electrodes pristine and soaked in 21 m LiTFSI solution.

particles can then easily react in these conditions to form, at the surface, a layer of TiO_2 (more than 10 nm thick, the probing depth of our XPS apparatus). The Ti2p core level spectrum, for the sample soaked in 21 m LiTFSI solution, shows very low TiO_2 contributions compared to the pristine electrode, indicating that once the electrode is soaked in WISE, a surface layer is covering the electroactive material. In the O1s core level spectrum of the pristine TiS_2 electrode (**Figure 10**a), the contributions are the same as for TiS_2 pristine powder.

When soaked in 21 m LiTFSI solution, the O1s core level spectrum is then dominated by LiTFSI salt contribution at 533.1 eV. Finally, in the F1s core level spectrum (Figure 10b), the pristine composite electrode shows only a -CF_2 contribution from the binder at 688 eV and no detectable presence of LiF, in contrast to the $LiFePO_4$ pristine electrode. For the electrode soaked in 21 m LiTFSI solution, two additional contributions are visible: -CF_3 at 689.1 and LiF at 685.5 eV. The CF_3/LiF ratio is 41/5, which is in the same order of magnitude as that observed in the LiTFSI F1s core level spectrum (90/10). This means that no additional layer of LiF is deposited on the TiS_2 surface other than that coming from salt degradation by X-ray irradiation. As for the S2p core level spectrum, not shown here, it displays only a weak signal of SO_4^{2-} species.

In summary, the soaking process of composite electrode materials in WISE is far from neutral with the development of a LiF-rich surface layer and a decomposition of TiS_2 into TiO_2-coated TiS_2. Thus, such a soaking process may influence the electrochemical performance of the materials. To assess this last point, we studied the electrochemical properties of the soaked electrodes in half-cell configuration versus Li metal, to determine the impact of the different surface layers on the electrochemical performance of both electroactive materials.

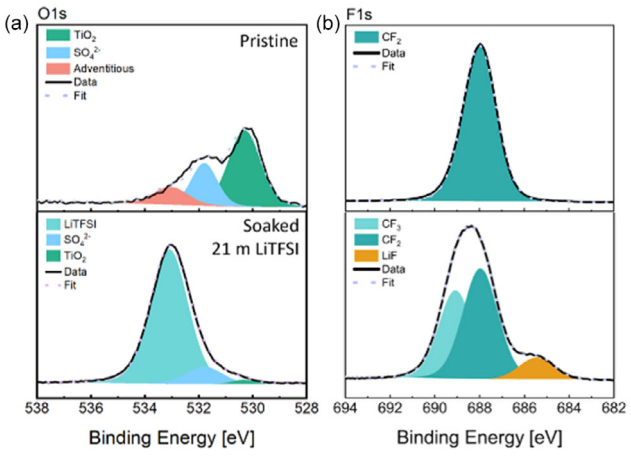

Figure 10. XPS core level spectrum of a) O1s and b) F1s obtained from TiS_2 pristine composite electrode and soaked in 21 m LiTFSI solution.

7. Evaluation of the Electrochemical Performance

7.1. Electrochemical Performance of $LiFePO_4$ Composite Electrode Soaked in WISE

Figure 11 displays the cycling profiles of $LiFePO_4$ composite electrodes (pristine and soaked) cycled in LP30-organic electrolyte with Li metal used as counter electrode. The typical potential plateau around 3.45 V vs. Li^+/Li is visible for all samples, showing at first sight no impact of the surface layer on the reaction mechanisms of $LiFePO_4$. As the surface layer developed with WISE is rather small and composed of LiTFSI salt, Li_2CO_3 and LiF, we did not expect drastic changes in the cycling profile of $LiFePO_4$ electrode.

Additional parameters from the electrochemical evaluation, are carefully investigated. The specific capacity, Coulombic efficiency and polarization of the four half-cells are presented in

Research Article
doi.org/10.1002/batt.202500539
Chemistry Europe
European Chemical Societies Publishing

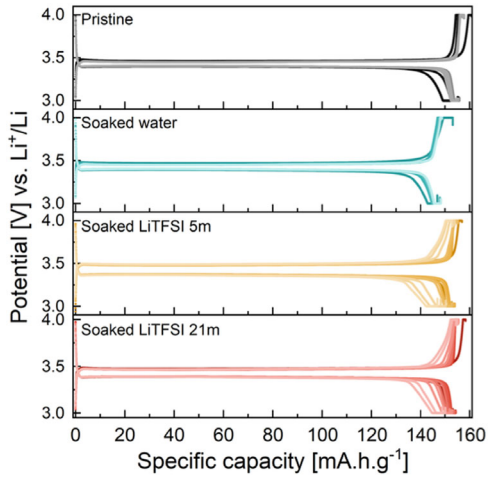

Figure 11. Cycling profiles of $LiFePO_4$ electrodes cycled in half-cell configuration (vs. Li^+/Li) in organic electrolyte LP30 at C/10 rate. The first 15 cycles are displayed using the following color code from darker (first cycle) to lighter color (last cycle).

Figure 12. As expected by the formation of lithium carbonate species, the water-soaked half-cell already presents the lowest specific capacity during the first cycle. As described above, soaking in water for 24 h leads to an increase in Li_2CO_3 content, indicating a loss of Li from $LiFePO_4$ composite electrode. Once the Li is lost (either in the solution or while creating lithium carbonate), the specific charge available is lowered. The capacity difference between the pristine and the water-soaked electrode is ≈8 mAh g^{-1}, corresponding to ≈5% of lithium loss, in agreement with Porcher et al.[39]

In early cycling stage, the electrodes soaked in 5 m LiTFSI solution and 21 m LiTFSI solution have a similar specific capacity to the pristine electrode (only slightly lower), indicating that the soaking process in LiTFSI solution prevented the electrode from degradation. In addition, as can be seen in Figure 12b, they possess the highest Coulombic efficiency during the first cycle, compared with the other cells. Here, two working hypotheses are proposed: i) it is known that during the first cycle, the low Coulombic efficiency is linked to the formation of passivation layers.[40,41] In our case, a LiF-rich surface layer could help to form a better CEI in organic electrolytes, especially as LiF is known to enhance the cycling performance,[42] and/or ii) as LiF has the tendency to dissolve in the electrolyte (especially at moderate concentration) and passivates the lithium metal electrode, it could improve the cycling properties of the Li metal counter electrode.[43] The presence of this layer can also be 'tracked' by monitoring the electrode polarisation (difference between charge and discharge potential plateau of $LiFePO_4$). As can be seen in Figure 12c, the polarization is highest for both electrodes soaked in WISE, indicating a high resistance in the cell probably linked to a surface layer on the top of the positive electrode and/or at the surface of the Li metal. After 10 cycles, the WISE-soaked electrodes performed worse in terms of specific capacity, Coulombic efficiency, and polarization. The charging specific capacity increases, whereas the discharge capacity falls, thus reducing the Coulombic efficiency. This is also the case for the pristine electrode but at a much slower rate. As the polarization increases, the layer at the electrode or lithium metal surface becomes thicker or more insulating. This indicates a chemical interaction between the surface layer developed with organic electrolyte and that developed by soaking in WISE, leading to the fast deterioration of the electrochemical performance.

7.2. Electrochemical Performance of TiS_2 Composite Electrode Soaked in WISE

Figure 13 displays the evolution of the electrochemical signature of TiS_2 half-cells during the first thirty-five cycles. The pristine electrode suffers from an important irreversible process during the first cycle, due to the formation of a SEI.[26] For the electrodes soaked in water or WISE, the irreversible process is more pronounced, indicating an additional process when the composite electrodes are soaked. A reasonable explanation is the presence/formation of TiO_2 (and/or oxysulfide) at the electrode surface as observed by XPS, although no electrochemical activity of TiO_2 is observed. Another explanation could be that the SEI developed during cycling could dissolved in organic electrolyte (during charge/discharge process) or chemically interact with the one generated by soaking, leading to a poorer electrochemical performance during cycling.

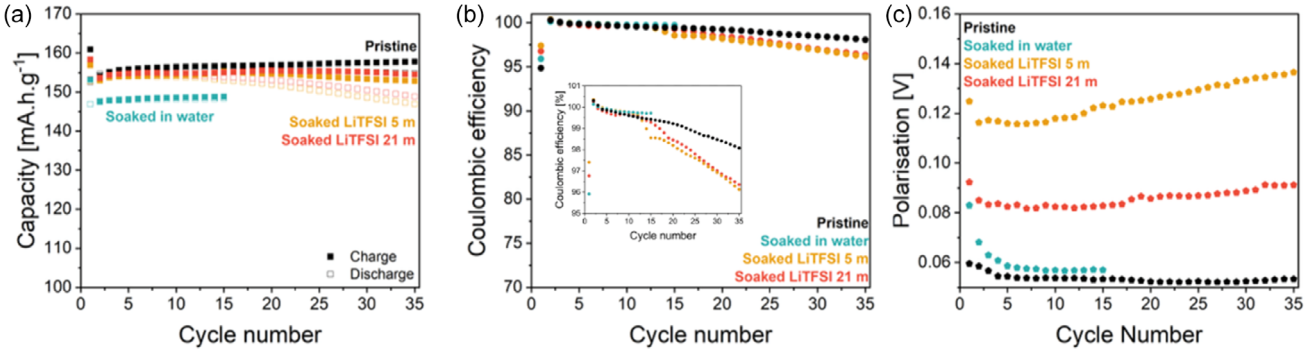

Figure 12. Electrochemical evaluation of $LiFePO_4$ composite electrolytes (pristine and soaked electrodes) cycled at C/10 in organic electrolyte vs. Li^+/Li. a) Specific capacities (charge and discharge), b) Coulombic efficiency, and c) Polarization (calculated at $x = 0.45$ state of charge).

Research Article
doi.org/10.1002/batt.202500539
Chemistry Europe
European Chemical Societies Publishing

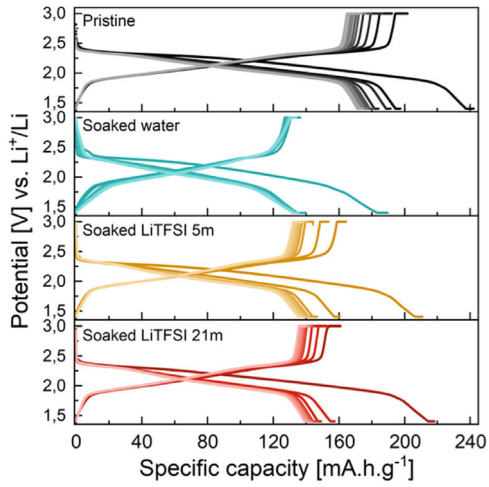

Figure 13. Cycling profiles of TiS_2 composite electrodes (pristine and soaked ones) cycled in half-cell configuration (vs. Li^+/Li) in organic electrolyte LP30 at C/10 rate. The first 15 cycles are displayed using the color code from darker (first cycle) to lighter color (last cycle).

Specific capacity, Coulombic efficiency and polarization are displayed in **Figure 14**. As it can be seen in Figure 14a, the pristine TiS_2 composite electrode reaches a specific capacity around 200 mAh g^{-1} (around 240 mAh g^{-1} expected theoretically, a value that could decrease if TiS_2 is replaced at the surface by TiO_2) after the first cycle, whereas electrodes soaked in WISE around 165 mAh g^{-1} and, the one soaked in water, ≈145 mAh g^{-1}. Soaking the composite electrode in aqueous electrolyte degrades the cycling performance, as at least 17% of the specific capacity is lost. This behavior is rather surprising, since the substitution of sulfur by oxygen leading to TiO_2 should not impact the electrochemical performance, as TiO_2 is generally a very stable material in organic electrolyte, despite some catalytic reaction with the organic electrolyte. However, cycling performance could be lowered if oxysulfides are generated.[44]

During the first cycles, the composite electrodes soaked in WISE seem to mitigate the degradation, but, after long-term cycling, the three soaked electrodes eventually reach the same specific capacity between 140 and 130 mAh g^{-1}, whereas the pristine electrode still achieves a specific capacity around 170 mAh g^{-1}. In terms of Coulombic efficiency (Figure 14b), water-soaked electrode has the lowest Coulombic efficiency during the first cycle (70%), whereas the pristine one reaches 83%. Eventually, the polarization was also analyzed at 60% state of charge, revealing a significant growth in the first cycles and then a linear evolution. The pristine and the electrodes soaked in 21 m LiTFSI solution show the lowest polarization, while that soaked in water has the highest one, which is reached after about 10 cycles before showing a linear growth like the other electrodes.

Unlike the $LiFePO_4$ electrode, TiS_2 composite electrodes are more impacted by the soaking processes (water or electrolyte solutions) since the specific capacity is drastically lowered when the sample is preliminary soaked. The reason behind this is the surface modification of TiS_2 into TiO_2 that leads to poorer electrochemical performance. However, it is interesting to see that the sample soaked in 21 m LiTFSI solution is less impacted and can achieve better electrochemical performance than the other soaked samples and has less polarization. This behavior is going in the direction that the sample is somehow protected by the surface layer.

8. Conclusion

To summarize the impact of soaking onto the active materials: 1) $LiFePO_4$ seems rather stable in an aqueous electrolyte without any degradation at the bulk level, whereas, at the surface, we noticed the formation of LiF indicating a little lithium depletion, maybe compensated by a lithium/proton exchange since Fe remains in the +II oxidation state. 2) TiS_2 is quite reactive when soaked in an aqueous environment. In fact, gas bubbles were observed when TiS_2 is in contact with aqueous environment, indicating a release of H_2S and the formation of TiO_2 (and/or oxysulfide) on the surface of the particles. This behavior seems to be buffered by high salt concentration, as less TiO_2 was detected at the surface of TiS_2 powder soaked in WISE compared to that soaked in water. TiS_2 composite electrodes no longer present sulfur species at their surface after prolonged exposure to air, as detected by XPS (and perhaps the elaboration process of the composite electrode also favors this). 3) Both electrodes are covered with a

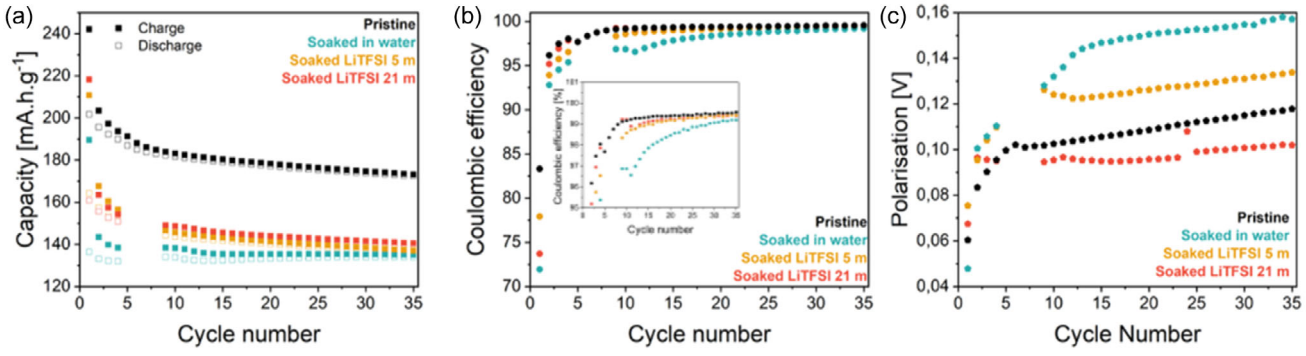

Figure 14. Electrochemical evaluation of TiS_2 composite electrolyte (pristine and soaked electrode) cycled at C/10 in inorganic electrolyte vs. Li^+/Li. a) Specific capacities (charge and discharge), b) Coulombic efficiency, and c) polarization (calculated at $x = 0.6$ state of charge).

surface layer on the top of the active particles, since the contributions of TiS_2 and $LiFePO_4$ were less visible in the XPS spectra, indicating that something is covering up the electrodes, either salt residue, oxide species and/or fluorinated species. 4) Soaking in water and WISE solutions impacted the cycling performance of both active materials in organic electrolytes. However, clear conclusions are difficult to draw since a passivation of the lithium metal counter electrode could also play a role.

This study allowed us to gain insight into the possible decomposition occurring in WISE when using electroactive materials. This detailed analysis will allow us to discriminate the effects coming from the contact between the materials (chemical reactions), from those happening during electrochemical processes, as will be discussed in second part of this study.

9. Experimental Section

Electrolyte Preparation

Lithium bis(trifluoromethanesulfonyl)imide (LiTFSI, $LiN(SO_2CF_3)_2$) was purchased from Solvionic and stored in an Ar-filed glovebox. LiTFSI electrolyte solutions of 21 and 5 mol kg^{-1} (hereafter referred as 21 and 5 m, respectively) were prepared by mixing LiTFSI salt and Milli-Q ultrapure water.

Electrode Elaboration

Composite electrodes were obtained by mixing 80 wt% of active materials ($LiFePO_4$ (LFP, MTI supplier) or TiS_2 (Sigma Aldrich, France) as active material), 10 wt% of carbon super C65 (Imerys), and 10 wt% of poly(vinylidene fluoride) (PVdF-kynar 900HSV, Arkema). The powders are grinded altogether by hand for at least 10 min prior adding then N-methylpyrrolidone (NMP) to solubilize the binder. The as-obtained slurry is then casted onto an aluminum foil, used as a current collector, by a doctor blade technique. The electrodes are then dried at 70 °C for 8 h. Once dried, the electrodes are punched in 12 mm diameter disk with an active material loading around 2.5 mg cm^{-2}. The porosity of the electrodes was estimated to be around 60%.

Cycling Tests

Coin cells are assembled in an Ar filled glovebox. Before cell assembly, the electrodes and the glass fiber separator (Whatman) are dried at 130 °C under dynamic vacuum. $LiFePO_4$ and TiS_2 composite electrodes are used as positive electrode, a glass-fiber separator is soaked with LP30 electrolyte 1/1 wt/wt dimethyl carbonate (DMC)/ ethylene carbonate (EC) and 1 M $LiPF_6$ (Solvionic), and lithium metal is used as counter electrode. The half cells are cycled at 25 °C in a temperature-controlled oven using galvanostatic cycling with potential limitation (GCPL) between 2.8 and 4 V versus Li^+/Li at a C/10 rate. Throughout the manuscript, all potentials are expressed against the Li metal counter electrode meaning versus Li^+/Li.

XPS Measurements

XPS spectra were obtained using a Thermo Scientific K-alpha spectrometer with a monochromated Al X-ray source (1486.6 eV, spot size 400 μm, constant angle of 90° between the sample surface and the analyzer). Pass energies of 30 and 100 eV were employed to record the core level and survey spectra, respectively. All spectra were acquired using an electron flood gun to compensate for possible positive charge accumulation during measurements. The obtained spectra are then deconvoluted and fitted using CasaXPS software with the Tougaard background type and calibrated using the C—C bound at 284.8 eV.[45]

XRD Measurements

XRD is used to determine the bulk structure of the electroactive materials. Lab-source XRD has been used for the investigation of the $LiFePO_4$ powder. Measurements were performed in capillaries using a copper K source on a Panalytical apparatus with a step size of 0.016° and a monochromator.

Synchrotron X-Ray Diffraction

They were performed at ID31 beamline at ESRF, Grenoble, France, was used for the investigation of the TiS_2 powder, due to the higher resolution in reciprocal space needed. An unfocused beam (50Q0 × 500 μm^2) at 68.044 keV ($\lambda = 0.1822$ Å) is used, in combination with a 2D detector (Dectris, Pilatus CdTe 2M). The 2D images are integrated into 1D XRD pattern using the pyFAI packages.[46]

Neutron Powder Diffraction Measurements

D2B high-resolution beamline two-axis diffractometer was used (Institut Laue-Langevin, Grenoble, France) to perform NPD measurements. Approximately 1 g of each samples (mentioned in the results section) was introduced in a Ø6.5 mm vanadium can. The diffractogram was collected at RT (approximatively 21 °C) in high intensity mode for 2 h. A Ge monochromator was used for the measurements, and the wavelength was determined to be 1.594 Å using $Na_2Ca_3Al_2F_{14}$ standard. Data were collected at ILL with Easy proposal acces.[47]

Mössbauer Spectroscopy

Transmission ^{57}Fe Mössbauer measurements were carried out at room temperature with a triangular velocity waveform. A Kr gas-filled was used for the detection of γ-rays produced by a 0.5 GBq 57Co:Rh source. Velocity calibration was carried out with an α-Fe foil at room temperature. Absorbers containing approximately 45 mg of electrode material and protected from air using thermally sealed plastic coffee bags, were used in all acquisitions. The experimental spectra were analyzed by least-square fitting with appropriate combinations of quadrupole doublets with Lorentzian profiles using the PC-Mos II computer program.[48]

Supporting Information

Supporting Information is available from the RSC website.

Acknowledgements

C.D. is grateful for the financial support provided by the IDEX project from the Université Grenoble Alpes. E.S. is greatly acknowledged for providing Easy proposal access for the measurement of samples on D2B beamline at ILL. The authors are

thankful to J.D. for providing in house beamtine and to M.M. for the measurement of the capillaries at ID31 beamline, ESRF (proposal ihma532). This research has benefited from the characterization equipment of the Grenoble INP–CMTC platform supported by the Centre of Excellence of Multifunctionnal Architectured Materials "CEMAM" (grant ANR-10-LABX-44−01) funded by "Investments for the Future Program." L.S. thanks the French National Research Agency for financial support through the Labex STORE-EX project (grant ANR-10-LABX-76–01). Moulay Tahar Sougrati is gratefully acknowledged for technical support in the measurement of the Mössbauer spectra.

Conflict of Interest

The authors declare no conflict of interest.

Author Contributions

Célia Doublet: formal analysis (lead); investigation (equal); methodology (equal); writing—original draft (equal); and writing—review and editing (supporting). **Ove Korjus**: formal analysis (lead); investigation (equal); writing—original draft (supporting); writing—review and editing (supporting). **Marta Mirolo**: formal analysis (equal); investigation (supporting); writing—original draft (supporting); and writing—review and editing (supporting). **Jakub Drnec**: formal analysis (supporting); investigation (supporting); and writing—review and editing (supporting). **Vincent Martin**: formal analysis (supporting); investigation (supporting); and writing—review and editing (supporting). **Emmanuelle Suard**: formal analysis (supporting); methodology (supporting); and writing review and editing (supporting). **Lorenzo Stievano**: formal analysis (supporting); investigation (supporting); and writing review and editing (supporting). **Lauréline Lecarme**: investigation (supporting); methodology (supporting); project administration (equal); supervision (lead); writing—original draft (supporting); and writing review and editing (supporting). **Claire Villevieille**: conceptualization (lead); formal analysis (equal); funding acquisition (lead); investigation (equal); methodology (lead); project administration (lead); supervision (lead); writing—original draft (lead); and writing—review and editing (lead).

Data Availability Statement

The data that support the findings of this study are available from the corresponding author upon reasonable request.

Keywords: electrochemical properties · Mössbauer spectroscopy · neutron powder diffraction · soaking processes · water-in-salt electrolyte · x-ray photoelectron spectroscopy

[1] W. Li, J. R. Dahn, D. S. Wainwright, *Science 264*, **1994**, 1115.
[2] L. Suo, O. Borodin, T. Gao, M. Olguin, J. Ho, X. Fan, C. Luo, C. Wang, K. Xu, *Science* **2015**, *350*, 938.
[3] S. F. Lux, L. Terborg, O. Hachmöller, T. Placke, H. W. Meyer, S. Passerini, M. Winter, S. Nowak, *J. Electrochem. Soc.* **2013**, *160*, A1694.
[4] M. McEldrew, Z. A. H. Goodwin, A. A. Kornyshev, M. Z. Bazant, *J. Phys. Chem. Lett.* **2018**, *9*, 5840.
[5] Y. Yamada, K. Usui, K. Sodeyama, S. Ko, Y. Tateyama, A. Yamada, *Nat. Energy* **2016**, *1*, 16129.
[6] L. Zhang, X. Hou, K. Edström, E. J. Berg, *Batteries Supercaps*, *5*, **2022**, e202200336.
[7] L. Coustan, G. Shul, D. Bélanger, *Electrochem. Commun.* **2017**, *77*, 89.
[8] N. Dubouis, P. Lemaire, B. Mirvaux, E. Salager, M. Deschamps, A. Grimaud, *Energy Environ. Sci.* **2018**, *11*, 3491.
[9] O. Borodin, L. Suo, M. Gobet, X. Ren, F. Wang, A. Faraone, J. Peng, M. Olguin, M. Schroeder, M. S. Ding, E. Gobrogge, A. von Wald Cresce, S. Munoz, J. A. Dura, S. Greenbaum, C. Wang, K. Xul, *ACS Nano* **2017**, *11*, 10462.
[10] L. Droguet, A. Grimaud, O. Fontaine, J.-M. Tarascon, *Adv. Energy Mater.* **2020**, *10*, 2002440.
[11] L. Droguet, M. Courty, O. Fontaine, J. M. Tarascon, A. Grimaud, *J. Electrochem. Soc.* **2022**, *169*, 070510.
[12] S. Ko, Y. Yamada, A. Yamada, *ACS Appl. Mater. Interfaces* **2019**, *11*, 45554.
[13] L. Suo, D. Oh, Y. Lin, Z. Zhuo, O. Borodin, T. Gao, F. Wang, A. Kushima, Z. Wang, H.-C. Kim, Y. Qi, W. Yang, F. Pan, J. Li, K. Xu, C. Wang, *J. Am. Chem. Soc.* **2017**, *139*, 18670.
[14] R. Bouchal, Z. Li, C. Bongu, S. L. Vot, R. Berthelot, B. Rotenberg, F. Favier, S. A. Freunberger, M. Salanne, O. Fontaine, *Angew. Chem., Int. Ed.* **2020**, *59*, 15913.
[15] R. Jommongkol, S. Deebansok, J. Deng, Y. Zhu, R. Bouchal, O. Fontaine, *Small* **2024**, *20*, 2303945.
[16] H. Zhang, D. Wang, C. Shen, *Appl. Surf. Sci.* **2020**, *507*, 145059.
[17] A. L. Bail, H. Duroy, J. L. Fourquet, *Mater. Res. Bull.* **1988**, *23*, 447.
[18] M. Cuisinier, J.-F. Martin, N. Dupré, A. Yamada, R. Kanno, D. Guyomard, *Electrochem. Commun.* **2010**, *12*, 238.
[19] M. Cuisinier, J.-F. Martin, N. Dupré, R. Kanno, D. Guyomard, *J. Mater. Chem.* **2011**, *21*, 18575.
[20] A. S. Andersson, B. Kalska, L. Häggström, J. O. Thomas, *Solid State Ion.* **2000**, *130*, 41.
[21] L. Aldon, A. Perea, M. Womes, C. M. Ionica-Bousquet, J. C. Jumas, *J. Solid State Chem.* **2010**, *183*, 218.
[22] A. S. Kamzin, A. V. Bobyl', E. M. Ershenko, E. I. Terukov, D. V. Agafonov, A. A. Valiullin, *Tech. Phys. Lett.* **2012**, *38*, 715.
[23] M. Bini, S. Ferrari, D. Capsoni, P. Mustarelli, G. Spina, F. D. Giallo, M. Lantieri, C. Leonelli, A. Rizzuti, V. Massarotti, *RSC Adv.* **2012**, *2*, 250.
[24] P. He, J.-L. Liu, W.-J. Cui, J.-Y. Luo, Y.-Y. Xia, *Electrochim. Acta* **2011**, *56*, 2351.
[25] H. Martinez, C. Auriel, D. Gonbeau, M. Loudet, G. Pfister-Guillouzo, *Appl. Surf. Sci.* **1996**, *93*, 231.
[26] L. Zhang, F. Kühling, A.-M. Mattsson, L. Knijff, X. Hou, G. Ek, T. Dufils, F. H. Gjørup, I. Kantor, C. Zhang, W. R. Brant, K. Edstrom, E. J. Berg, *ACS Energy Lett.* **2024**, *9*, 959.
[27] W. Sun, L. Suo, F. Wang, N. Eidson, C. Yang, F. Han, Z. Ma, T. Gao, M. Zhu, C. Wang, *Electrochem. Commun.* **2017**, *82*, 71.
[28] G. Greczynski, L. Hultman, *Prog. Mater. Sci.* **2020**, *107*, 100591.
[29] Y. Bi, T. Wang, M. Liu, R. Du, W. Yang, Z. Liu, Z. Peng, Y. Liu, D. Wang, X. Sun, *RSC Adv.* **2016**, *6*, 19233.
[30] W. Xiong, Q. Hu, S. Liu, *Anal. Methods* **2014**, *6*, 5708.
[31] C. Gao, J. Zhou, G. Liu, L. Wang, *Appl. Surf. Sci.* **2018**, *433*, 35.
[32] K. Sun, Q. Zhang, D. C. Bock, X. Tong, D. Su, A. C. Marschilok, K. J. Takeuchi, E. S. Takeuchi, H. Gan, *J. Electrochem. Soc.* **2017**, *164*, A1291.
[33] J. C. Dupin, D. Gonbeau, I. Martin-Litas, P. Vinatier, A. Levasseur, *Appl. Surf. Sci.* **2001**, *173*, 140.
[34] G. Beamson, D. Briggs, *J. Chem. Ed.* **1993**, *70*, A25.
[35] D. Ensling, M. Stjerndahl, A. Nytén, T. Gustafsson, J. O. Thomas, *J. Mater. Chem.* **2009**, *19*, 82.
[36] K. N. Wood, G. Teeter, *ACS Appl. Energy Mater.* **2018**, *1*, 4493.
[37] M. Paillot, A. Wong, S. A. Denisov, P. Soudan, P. Poizot, B. Montigny, M. Mostafavi, M. Gauthier, S. L. Caër, *ChemSusChem* **2023**, *16*, e202300692.
[38] H.-G. Steinrück, C. Cao, M. R. Lukatskaya, C. J. Takacs, G. Wan, D. G. Mackanic, Y. Tsao, J. Zhao, B. A. Helms, K. Xu, O. Borodin, J. F. Wishart, M. F. Toney, *Angew. Chem., Int. Ed.* **2020**, *59*, 23180.
[39] W. Porcher, P. Moreau, B. Lestriez, S. Jouanneau, D. Guyomard, *Electrochem. Solid-State Lett.* **2008**, *11*, A4.
[40] Y.-D. Cho, G. T.-K. Fey, H.-M. Kao, *J. Power Sources* **2009**, *189*, 256.
[41] A. Tron, Y. N. Jo, S. H. Oh, Y. D. Park, J. Mun, *ACS Appl. Mater. Interfaces* **2017**, *9*, 12391.

[42] T. Lei, L. Xue, Y. Li, Y. Chen, J. Zhu, S. Deng, X. Lian, G. Cao, W. Li, *Ceram. Int.* **2019**, *45*, 18106.
[43] J. Ko, Y. S. Yoon, *Ceram. Int.* **2019**, *45*, 30.
[44] S. Sallard, E. Castel, C. Villevieille, P. Novak, *J. Mater. Chem. A.* **2015**, *3*, 16112.
[45] N. Fairley, V. Fernandez, M. Richard-Plouet, C. Guillot-Deudon, J. Walton, E. Smith, D. Flahaut, M. Greiner, M. Biesinger, S. Tougaard, D. Morgan, J. Baltrusaitis, *Appl. Surface Sci. Adv.* **2021**, *5*, 100112.
[46] J. Kieffer, J. P. Wright, *Powder Diffr.* **2013**, *28*, S339.
[47] https://doi.ill.fr/10.5291/ILL-DATA.EASY-1328.
[48] G. Gross, *PC-Mos II, v. 1.0. Manual and Program Documentation*, Technische Universitaet Muenchen, Munich, Germany **1993**.

Manuscript received: August 1, 2025
Revised manuscript received: August 26, 2025
Version of record online: